Molecular Therapy
Nucleic Acids
Original Article

Royal jelly extracellular vesicles promote wound healing by modulating underlying cellular responses

Simón Álvarez,[1,7] Pamina Contreras-Kallens,[1,7] Sebastian Aguayo,[2,3,7] Orlando Ramírez,[1] Catalina Vallejos,[4] Jorge Ruiz,[4] Eva Carrasco-Gallardo,[5] Stefanie Troncoso-Vera,[5] Bernardo Morales,[6] and Christina M.A.P. Schuh[1]

[1]Centro de Medicina Regenerativa, Facultad de Medicina, Clínica Alemana-Universidad del Desarrollo, Santiago, Chile; [2]Dentistry School, Faculty of Medicine, Pontificia Universidad Católica de Chile, Santiago, Chile; [3]Institute for Biological and Medical Engineering, Schools of Engineering, Medicine and Biological Sciences, Pontificia Universidad Católica de Chile, Santiago, Chile; [4]Laboratorio de Medicina Experimental, Facultad de Medicina, Clínica Alemana-Universidad del Desarrollo, Santiago, Chile; [5]Laboratorio de Histopatología, Cemesi, Santiago, Chile; [6]Facultad de Salud, Universidad del Alba, Santiago, Chile

***Apis mellifera* royal jelly (RJ) is a well-known remedy in traditional medicine around the world and its versatile effects range from antibacterial to anti-inflammatory properties and pro-regenerative properties. As a glandular product, RJ has been shown to contain a substantial number of extracellular vesicles (EVs), and, in this study, we aimed to investigate the extent of involvement of RJEVs in wound healing-associated effects. Molecular analysis of RJEVs verified the presence of exosomal markers such as CD63 and syntenin, and cargo molecules MRJP1, defensin-1, and jellein-3. Furthermore, RJEVs were demonstrated to modulate mesenchymal stem cell (MSC) differentiation and secretome, as well as decrease LPS-induced inflammation in macrophages by blocking the mitogen-activated protein kinase (MAPK) pathway. *In vivo* studies confirmed antibacterial effects of RJEVs and demonstrated an acceleration of wound healing in a splinted mouse model. This study suggests that RJEVs play a crucial role in the known effects of RJ by modulating the inflammatory phase and cellular response in wound healing. Transfer of RJ into the clinics has been impeded by the high complexity of the raw material. Isolating EVs from the raw RJ decreases the complexity while allowing standardization and quality control, bringing a natural nano-therapy one step closer to the clinics.**

INTRODUCTION

Despite many advances in regenerative medicine, wound infection by bacteria remains an important problem that negatively affects the clinical outcome of surgical procedures.[1] Especially chronic wounds are prone to complications, such as excessive inflammation, persistent infections, formation of drug-resistant microbial biofilms, and the inability of dermal and/or epidermal cells to respond to reparative stimuli (reviewed by Frykberg and Banks[2]). Over the last decades, extracellular vesicles (EVs) have become increasingly used in the field of nano-medicine. After key findings such as their role in the expression of antigens[3] and ability to transfer mRNA/miRNA,[4] they are now established as one of the main factors in intercellular communication. Interestingly, it has been shown that EVs are capable of interspecies and interkingdom communication, with a wide range of therapeutic applications.[5]

Several honeybee products, such as honey and royal jelly (RJ), have been used since ancient times in various cultures for their antimicrobial and pro-regenerative properties (summarized in Moore and Ahmed et al.[6,7]). More recently, advances have been made to analyze the effects of RJ in controlled environments and on a molecular basis. Several active compounds have been found, among those major RJ proteins (MRJPs), apisimin, royalisin, jelleins, defensins, apolipophorin-III-like, and glucose oxidase.[8] Pre-clinical studies described ameliorating effects of RJ in several conditions, such as mucositis, colitis, bone formation, and infected ulcers[9–12] or diabetic foot ulcers.[13] On a cellular level, RJ has been found to induce osteogenesis and exert anti-inflammatory properties in periodontal ligament cells, promote neurogenesis in neural stem cells, and increase migration of human dermal fibroblasts.[14–16] Several studies have described the immune-modulatory properties of RJ and its components.[17–19] Furthermore, the antibacterial properties of RJ were first shown in 1939 by McClesky et al., demonstrating a bactericidal effect on *Escherichia coli*, *Eberthella thyphosa*, and *Staphylococcus aureus*.[20]

Recently, our group was the first to discover the presence of EVs as a new active part of RJ that demonstrated antibacterial and biofilm-inhibiting properties against *S. aureus*.[21] Furthermore, RJ-derived EVs (RJEVs) were found to integrate into mammalian cells and increase cellular migration in mesenchymal stem cells (MSCs)[21] and dermal fibroblasts,[22] confirming effects previously described for crude RJ.[16] The discovery that these vesicles display functional effects on

Received 29 September 2022; accepted 10 February 2023;
https://doi.org/10.1016/j.omtn.2023.02.008.

[7]These authors contributed equally

Correspondence: Christina Schuh, Clínica Alemana-Universidad del Desarrollo, Avenida Plaza 680, Las Condes, Santiago de Chile.
E-mail: cschuh@udd.cl

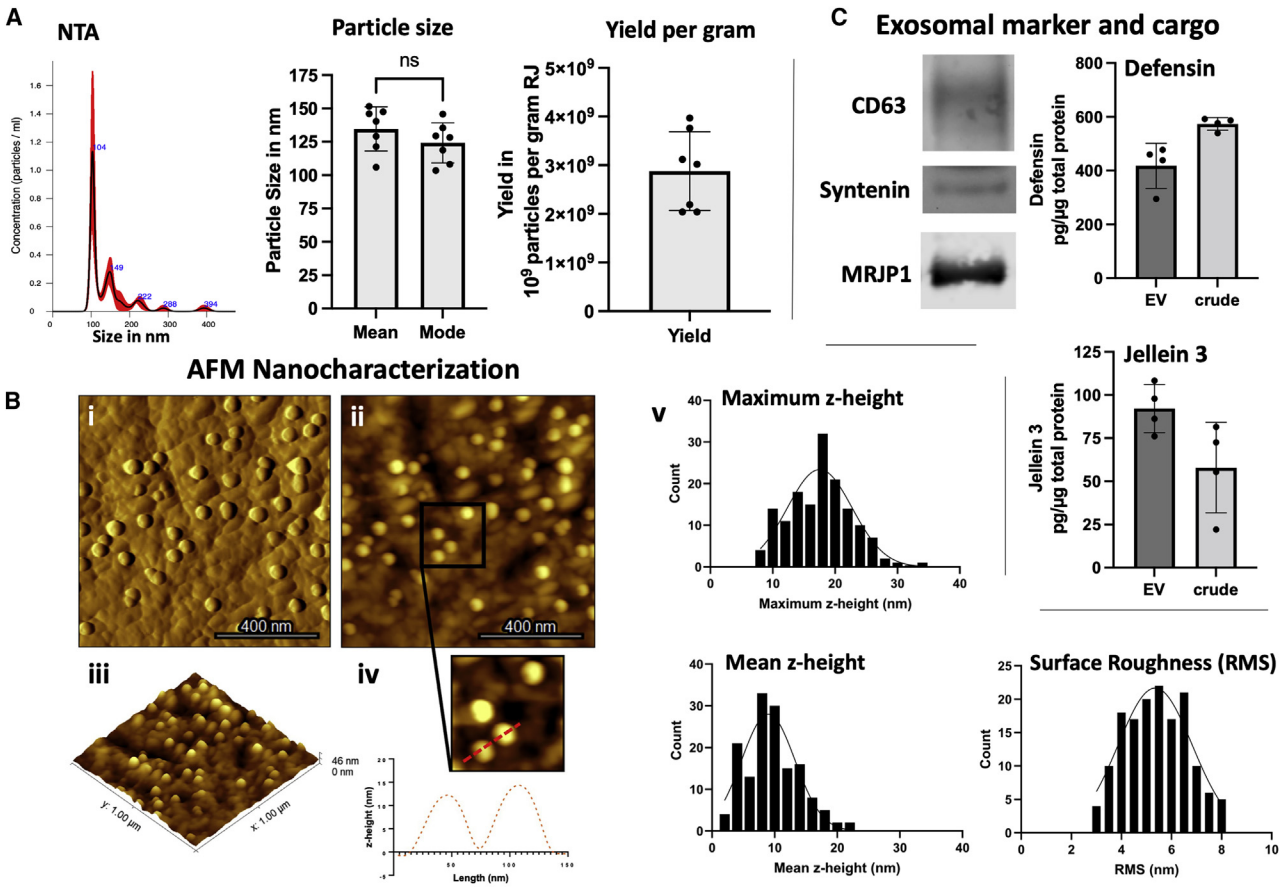

Figure 1. Morphological and biochemical characterization of RJEVs

(A and B) (A) Representative NTA histogram; average (mean) and median (mode) particle size in nanometers (*p < 0.05; Student's t test); particle yield of RJEV per gram raw RJ; n = 7. (B) AFM-based analysis of RJEV vesicle shape; (i) amplitude, (ii) height, and (iii) 3D height reconstruction of RJEV immobilized onto PLL-coated mica. (iv) Profile trace obtained on two RJEVs demonstrating their shape and size. (v) Maximum and mean heights and RMS surface roughness of immobilized RJEV (n = 150). (C) Western blot analysis of exosomal markers. CD63, Syntenin-1 and RJEV cargo MRJP-1; n = 3; ELISA analysis of RJEV cargo Defensin-1 and Jellein-3; n = 4. Data are shown as mean ± SD.

mammalian cells allows hypothesizing that RJEVs might be involved in several of the known biological effects of RJ, given their known capacity to shuttle cargo into cells and exert intracellular effects. Therefore, in the current study, we investigated potential routes of entry into mammalian cells, modulatory effects on MSCs, anti-inflammatory effects of RJEVs, and translatability into an *in vivo* wound healing model.

RESULTS

RJEV characterization and uptake analysis

Before functional experiments, we performed an in-depth characterization of RJEVs utilized in this study. Isolated RJEVs were found to display a mean size of 134.5 ± 16.5 nm and a median size of 124.2 ± 14.9 nm, demonstrating RJEV homogeneity within the samples. No significant differences were found between the mean and median RJEV sizes. Particle yield was between 3.9×10^9 and 2.1×10^9 particles per gram of raw material, which is in line with previous observations (Figure 1A).[21] Furthermore, we utilized atomic force microscopy (AFM) to characterize the ultrastructure of mica-immobilized RJEVs, confirming vesicle shape and integrity at the nanoscale in both height and amplitude images (Figure 1B). Also, RJEVs were found to display a maximum height (17.6 ± 4.9 nm) and mean height (9.7 ± 4.2 nm), consistent with the expected morphology of mica-bound EVs, and an average root-mean-square (RMS) surface roughness of 5.4 ± 1.2 nm.

The exosomal origin of RJEVs was confirmed by verifying the presence of CD63 and syntenin, two conserved exosomal markers present in *Apis mellifera* (Kyoto Encyclopedia of Genes and Genomes [KEGG]: exosome, *A. mellifera*, entry 552721 CD63; entry 551650 syntenin). Cross-species reactivity for CD63 is shown in Figure S1. Furthermore, the relevant cargo proteins MRJP-1, defensin-1, and jellein-3 were also identified within RJEVs.

To study uptake mechanisms, the specific inhibitors amiloride, omeprazole, filipin III, and chlorpromazine were used to assess the role of

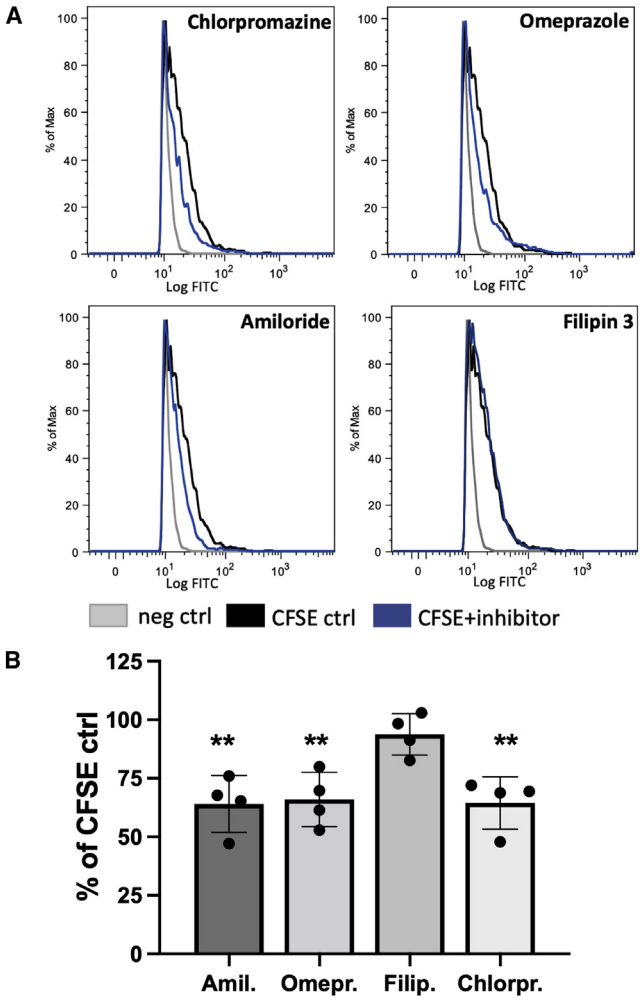

Figure 2. Route of RJEV uptake into human MSCs

(A) Flow cytometry histograms of MSCs without RJEV (neg control, negative control; gray), incubated with CFSE-RJEV (CFSA control, black) and with CFSE-RJEV and the respective inhibitor (blue, CFSE + inhibitor) chlorpromazine, omeprazole, amiloride, and filipin 3. (B) Quantitative analysis of RJEV uptake inhibition into MSCs, displayed as a percentage of respective CFSE-RJEV control; n = 4, (*$p < 0.05$; **$p < 0.01$; one-way ANOVA with Tukey's post hoc). Data are shown as mean ± SD.

macropinocytosis, membrane fusion, lipid raft or caveolae-mediated endocytosis, and clathrin-dependent endocytosis, respectively. Amiloride, omeprazole, and chlorpromazine significantly decreased uptake of CFSE-RJEVs into MSCs, to similar extents (64% ± 12.15%, 65.9% ± 11.6%, 64.51% ± 11.2%). However, filipin III did not exert significant inhibitory effects on CFSE-RJEV uptake (94.9% ± 8.8%), indicating a minor role of lipid rafts in RJEV internalization (Figure 2).

Effect of RJEVs on MSC differentiation, population doubling time, and secretion

As a next step, MSC cultures derived from adipose tissue of healthy donors were analyzed for *in vitro* chondrogenic, osteogenic, and adipogenic differentiation potential, either pretreated or in the presence of RJEVs (Figures 3A and 3B). Chondrogenic differentiation was confirmed with Safranin O staining, and both qualitative and quantitative analysis showed a significant increase (25%–40%) of proteoglycan deposition in the RJEV group compared with control; however, no effect was observed in the pre-treatment group. Interestingly, Alizarin red stain for calcium after osteogenic induction was increased in both groups, with RJEV displaying a highly reproducible effect of around a 50% increase compared with the untreated control. Pre-treatment resulted in an increase of 10%–130% compared with control. Furthermore, adipogenic differentiation analyzed by oil red O was significantly decreased in the RJEV group compared with the untreated control. Pre-differentiation, comparable with osteogenic differentiation, led to a higher spread within the data and a less predictable outcome. While three out of four donors displayed a decrease in adipogenic differentiation, one donor in the pre-treatment group displayed an increase (Figures 3A and 3B).

Subsequently, population doubling time (PDT) was observed over a time period of 10 passages (P3–P12) (Figure 3C). In the control group, a continuous increase in PDT after P3 was observed. In P8–P12, PDT was significantly higher compared with P3. In the RJEV group, while initial PDT was higher in P3–P6, the PDT remained approximately the same over the course of 10 passages (5.6 ± 0.5 days, compared with control 6 ± 1.6 days and RJEV preconditioning 6.37 ± 1.7 days). Interestingly, MSCs preconditioned with RJEVs displayed a PDT similar to RJEVs in P3, subsequently decreased in P4 and P5, and finally increased to levels comparable with the control group, indicating a transitory effect of RJEV preconditioning on proliferation.

Aside from the potential of MSCs to differentiate into specific lineages, their secretory profile has also been shown to be highly important (Figure 3D). Therefore, we assessed the influence of RJEVs on the secretion of four factors known to be involved in wound healing, and found that insulinlike growth factor (IGF) (133.65 ± 32.63 ng to 320.36 ± 28.77 ng/10^5 cells), hepatocyte growth factor (HGF) (49.9 ± 11.21 ng to 136.22 ± 34.34 ng/10^5 cells), and vascular endothelial growth factor (VEGF) (31.86 ± 6.8 ng to 47.87 ± 10.88 ng/10^5 cells) were significantly increased in the RJEV group. Finally, there also was a tendency toward a higher secretion of bFGF in the presence of RJEVs. However, the results were not statistically significant.

Immune-modulatory effect of RJEVs

RJ has been previously described as anti-inflammatory; however, it is unknown how RJEVs are involved in this effect. Hence, we stimulated the macrophage cell line RAW 264.7 with lipopolysaccharide (LPS) and subsequently analyzed the secretion of the pro-inflammatory cytokines interleukin (IL)-1β, IL-6, and tumor necrosis factor alpha (TNFα). RJEVs in the absence of LPS did not trigger the increased secretion of pro-inflammatory cytokines, indicating that RJEVs alone are not pro-inflammatory (Figure 4A). LPS significantly increased the secretion of all three pro-inflammatory cytokines assessed. The presence of higher-dose RJEVs (10^7 RJEVs) during LPS stimulation significantly decreased the amount of secreted IL-1β, IL-6, and

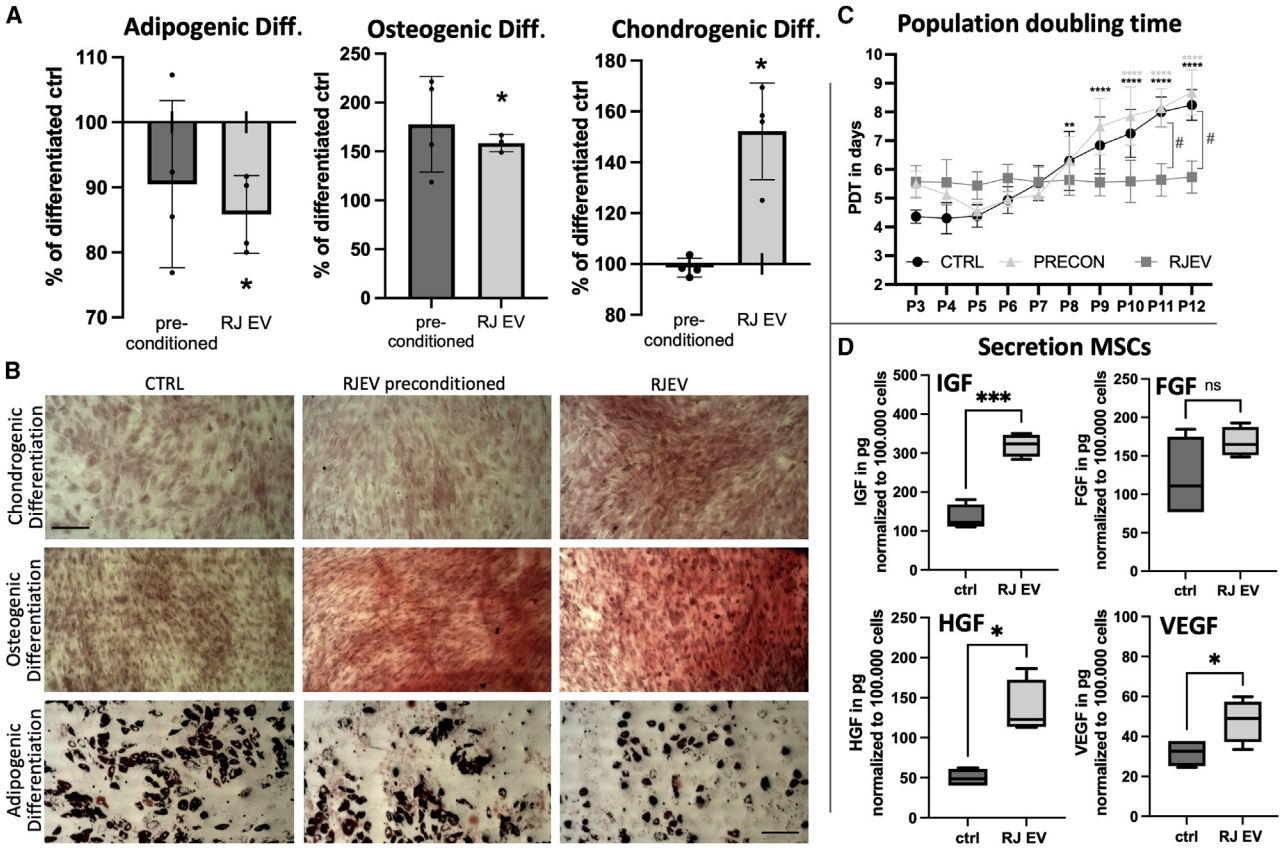

Figure 3. Effects of RJEVs on human MSCs

(A–C) (A and B) Differentiation into adipogenic, osteogenic, and chondrogenic lineage. (A) Quantification of differentiation in RJEV preconditioned group (dark gray) and RJEV group (light gray), displayed as percentage of untreated differentiated control (≙ 100%); n = 4, with technical duplicates; statistical significance tested with one-way ANOVA with Tukey's post hoc; *p < 0.05. (B) Representative images of MSC differentiation after 14-day induction and with oil red O (adipocytes), Alizarin red (osteocytes), and Safranin O (chondrocytes); scale bar ≙ 100μm. (C) Population doubling time of MSCs; seeded at 3.3×10^3 per cm^2, passaged and counted every 120 h (5 days); calculation, PDT in days = ((time in days) × log(2))/(log (final cell number) × log (initial cell number)); groups, untreated control (black, circle), RJEV preconditioned MSCs (light gray, triangle), and RJEV (dark gray, square). Significance tested with two-way ANOVA and Šídák's multiple comparisons test; *p < 0.05; **p < 0.01, ***p < 0.001, ****p < 0.0001, of respective group compared with P3; #p < 0.05, between groups within the same passage. (D) Secretory profile of MSCs in the presence of RJEV; levels of IGF-1, FGF, HGF, and VEGF in supernatants measured with ELISA; secretion normalized to 100,000 cells. N = 4; significance tested with students t test; *p < 0.05; **p < 0.01, ***p < 0.001. For A and C data are shown as mean ± SD. For D data are shown as box plot with mean ± min/max and quartiles.

TNFα (56.32%, 58.08%, and 63.04% decrease compared with LPS control, respectively). Lower dose (10^5 RJEVs) displayed significant effects in IL-6 and TNFα secretion (15.99% and 24.58% decrease), however, not in the secretion of IL-1β (9.8%). (Figure 4A).

Finally, western blot analysis of JNK and ERK1/2 revealed a strong response of both to LPS, expressed in the phosphorylation of both proteins. In a dose-dependent manner, RJEVs significantly decreased phosphorylation, indicating involvement of RJEVs in the mitogen-activated protein kinase (MAPK) pathway (Figures 4B i and 4B ii).

In vivo *antibacterial properties*

The antibacterial properties of RJEVs were demonstrated by our group previously in several studies under controlled *in vitro* conditions; however, this effect had not yet been confirmed in an *in vivo* model. To create controlled conditions, a subcutaneous pouch model was chosen to avoid cross-contamination with other bacterial strains, wound cleaning, and systemic infection, among others. Colony count after 48 h *in vivo* and subsequent 24 h of cultivation on BHI agar revealed around 8.0×10^7 colony-forming units (CFU) in the *S. aureus* control group and 7.62×10^7 CFU in the *S. aureus* collagen gel group (Figure 5B). Most importantly, no bacteria were detected in the control group without *S. aureus* and the *S. aureus* RJEVs collagen gel group. This result was confirmed by viability tests in a microwell plate and resazurin, demonstrating a bactericidal effect of RJEVs released by collagen gels *in vivo* (Figure 5C) due to the irreversibility of the effect.

In vivo *wound healing assay*

Finally, the effect of RJEVs on epithelial regeneration was assessed in a full-thickness wound mouse model. After infliction, wounds were

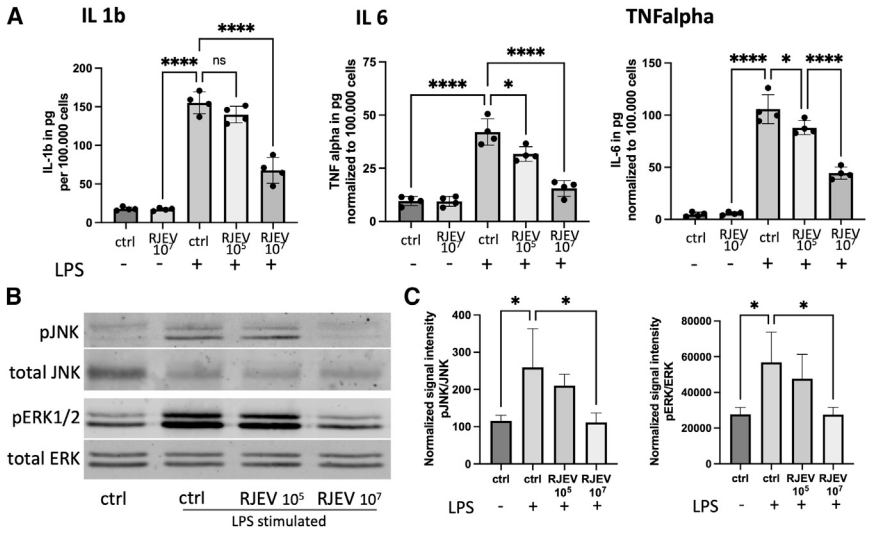

Figure 4. Immune-modulatory effect of RJEVs

(A) Secretion of pro-inflammatory cytokines IL-1, IL-6, and TNFα from RAW 264.7 macrophages after stimulation with LPS, measured with ELISA; secretion was measured in cells without LPS stimulation and treatment (control, LPS−), in the presence of RJEV (RJEV 10^7, LPS−), stimulated with LPS (control, LPS+), with a low dose of RJEV (RJEV 10^5, LPS+), and a high dose of RJEV (RJEV 10^7, LPS+); results were normalized on 100,000 cells; n = 4. (B) (i) Western blot analysis of phosphoERK/ERK 1/2, and phosphoJNK/JNK expression in RAW 264.7 macrophages of treated with RJEV 10^5 and RJEV 10^7, stimulated with LPS, compared with untreated and unstimulated control, visualized with Odyssey. (B) (ii) Quantification of phosphoERK 1/2 relative to ERK 1/2 and phosphoJNK relative to JNK in respective groups; n = 4. Significance for (A) and (C) was tested with one-way ANOVA with Tukey's post hoc; *p < 0.05, **p < 0.01, ***p < 0.001, ****p < 0.0001. Data are shown as mean ± SD.

covered with collagen hydrogels with and without RJEVs and wound closure was documented every 5 days. RJEVs significantly accelerated wound healing in the first 10 days, compared with collagen and untreated control (Figures 5B i and 5B ii); however, on day 15, all wounds were completely closed, and no difference could be observed on a macroscopic level. Furthermore, no important differences in vascularization were observed between the groups. Nevertheless, inflammatory cell and epithelization quantification showed that RJEVs significantly improved wound healing on a cellular level (Figures 6Ci and 6Cii).

DISCUSSION

EVs derived from non-mammalian sources have become increasingly interesting in the last decade as a potential tool for standardizing natural medical treatments.[5] However, the characterization of novel non-mammalian EV sources and EVs has been proved complex due to the absence of classical exosomal markers and the need to find validated alternatives, workarounds, and novel criteria. Our group first reported honeybee EVs in a preliminary study that assessed vesicle shape and internalization into mammalian cells.[21] Particle characterization and quantification for this study revealed a relatively pure EV population, with no significant secondary populations (Figure 1A). Verification of vesicle shape was previously performed using transmission electron microscopy.[21] However, while this method displays several advantages, such as broad availability and easy-to-use protocols, it lacks further insight into particle characteristics such as height and surface structure. Furthermore, electron microscopy involves destructive sample preparation (e.g., counterstaining, vacuum) that can alter the ultrastructural morphology and properties of EVs. Therefore, here we utilized AFM in tapping mode to gain information on RJEV shape and ultrastructural morphology with minimal sample destruction under environmental conditions. At the nanoscale, RJEVs display similar sizes, shapes, and morphological characteristics as other EVs and exosomes from diverse sources previously described in the literature.[23–25] Overall, AFM quantitative analysis showed an average maximum height of 17.6 ± 4.9 nm and a mean height of 9.7 ± 4.2 nm for RJEVs. Furthermore, a homogeneous nanoscale surface roughness was observed across all studied RJEVs (mostly ranging between 4 and 7 nm). As vesicle surface roughness is mostly determined by membrane composition,[26] particle roughness analysis may serve as a reference value for future EV studies utilizing mammalian or non-mammalian sources.

To determine the origin of EVs, classical cytosomal and membrane markers associated with the endosomal sorting complex required for transport (ESCRT) machinery are commonly analyzed. However, both the ESCRT-dependent and ESCRT-independent pathways have been mainly characterized for mammalian cells,[27] while, for example, insect and plant mechanisms have yet to be elucidated. Therefore, we assessed the potential exosomal origin of RJEVs by employing the KEGG to identify candidate proteins for *A. mellifera*. CD63 and syntenin (KEGG: exosome, *A. mellifera*, entry 552721 CD63; entry 551650 syntenin), which are crucial for ESCRT machinery were both found in the RJEV samples (Figure 1C). Syntenin is known to recruit CD63 in early endosome formation,[28,29] indicating a potential exosomal origin of the isolated RJEVs. Nevertheless, further studies are needed to identify the exosome biogenesis and release mechanism in honeybees, since several well-known components have been described in *A. mellifera*, such as ESCRT-I, II, or syndecan (KEGG: *A. mellifera*; entry 551408, 410869, 413557), but several others, such as ESCRT-III or ALIX, are missing.

As mentioned above, our previous studies reported the uptake of RJEVs into mammalian cells, which we further investigated in this study. We hypothesized an uptake of RJEVs dependent on macropinocytosis or endocytosis, since the differences in membrane composition between mammalian cells and honeybee cells are significant in terms of composition (e.g., presence of bee-specific fatty acids

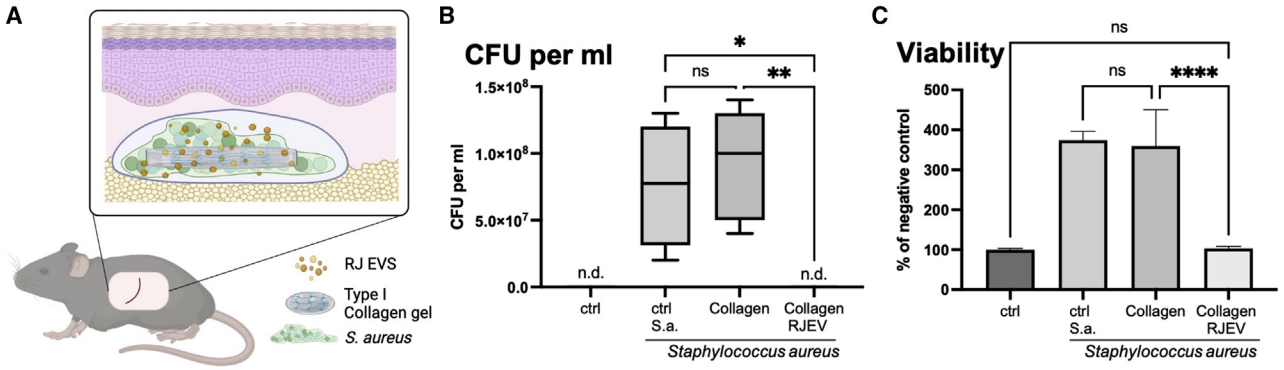

Figure 5. RJEV antibacterial activity in an *in vivo* mouse model

(A) Schematic of the animal model utilized to assess antibacterial activity. In 10- to 12-week-old C57BL6 mice, a subcutaneous pocket was created, and *S. aureus* ATCC 25923 were incubated in with type I collagen gels containing 5×10^9 RJEV/mL, compared with sham control, untreated control, and collagen gel control without RJEVs. The collagen gel releases RJEVs over time, which exerts an antibacterial effect, evaluated after 48 h *in vivo*. (B) Quantification of colony forming units (CFU) per milliliter; n.d., not detected. Data are shown as box plot with mean ± min/max and quartiles. (C) Viability measured with resazurin assay in sham, *S. aureus* control, collagen, and collagen RJEVs; n = 4–6. Data are shown as mean ± SD. Significance for (B) and (C) was tested with one-way ANOVA with Tukey's post hoc; *p < 0.05, **p < 0.01, ***p < 0.001, ****p < 0.0001.

such as 10-hydroxy-2-decenoic acid (10-HDA)[30]) and may not facilitate membrane fusion. Interestingly, we found membrane fusion as well as macropinocytosis and clathrin-dependent endocytosis to be involved in RJEV uptake into mammalian cells (Figure 2). This indicates a dual effect of RJEVs in mammalian cells: on the one hand, a direct release of RJEV cargo (e.g., MRJP-1, defensin-1, jellein-3; Figure 1C) into the cytoplasm after membrane fusion, and, on the other hand, intracellular sorting following internalization via other mechanisms. Interestingly, lipid raft-mediated endocytosis (blocked by filipin III) appeared not to be part of the RJEV uptake mechanism (Figure 2), which might be explained by missing interactions of honeybee-specific fatty acids as well as other membrane components with mammalian cell lipid rafts.

RJ has a long-standing history of medical applications, especially in accelerating wound healing,[9–12,31] as well as displaying anti-microbial[32–37] and anti-inflammatory effects.[17] The underlying effects have been attributed to a number of effects, including royalactin, also known as MRJP-1, contributing to increasing multipotency of mammalian stem cells.[38] Since we could verify the presence of MRJP-1 within RJEVs, we subsequently assessed their potential effect on MSCs, which are a crucial part of the wound healing process. Analyzing general *in vitro* characteristics such as PDT and multi-lineage differentiation, we found different stimulating and inhibiting effects. Adipogenesis and osteogenesis are known antagonistic MSC differentiations. Continuous exposure to RJEVs strongly increased osteogenic differentiation while decreasing adipogenic differentiation. Preconditioning MSCs with RJEVs had a similar tendency; however, the effect was not significant. Interestingly, chondrogenic differentiation was not influenced by preconditioning with RJEVs but significantly increased when continuously exposed to RJEVs. These results indicate that no increase in the multipotency of MSCs can be observed, since not all three lineages are increased in a similar manner, as described for, e.g., extracorporeal shockwave treatment in MSCs.[39] PDT increased over time in the control and RJEV preconditioned groups (after an initial decrease), which is a known effect in MSCs.[40,41] RJEVs had a preserving effect on MSC proliferation over time, with no significant changes in PDT, and the potential underlying effects should be investigated in future studies.

Most interesting for wound healing is the secretory profile of MSCs, since tissue-resident MSCs modulate the wound bed by secreting a variety of proteins. Among the most important ones are (1) IGF, a chemotactic agent for endothelial cells that stimulates hyaluronan as well as increasing fibroblast and keratinocyte migration[42]; (2) fibroblast growth factor (FGF), which displays an anti-fibrotic effect by decreasing myofibroblast differentiation and fibronectin[43,44]; (3) HGF, which increases migration, proliferation, and matrix metalloproteinase production of keratinocytes and also increases dedifferentiation of epidermal cells[45–47]; and (4) VEGF, which increases angiogenesis, collagen deposition, and epithelization.[48] Overall, RJEVs significantly increased IGF, HGF, and VEGF secretion, but not FGF, indicating a more pro-angiogenic and pro-migratory effect in wound healing, and only minor effects on scarring and fibrosis.

Furthermore, the anti-inflammatory effect of RJ has previously been described in several studies[17,49,50] and has subsequently been attributed to three RJ-specific fatty acids (10-hydroxydecanoic acid [10-H2DA], *trans*-10-hydroxy-2-decenoic acid [10-HDAA], and 1,10-decanedioic acid [SEA]) that modulate the MAPK pathway.[50] Interestingly, the observed inhibiting effects were minimal compared with the fatty acid dose applied. The content of 10-H2DA in RJ is between 1.5% and 2.5%.[51] Chen et al. utilized 2.5–5 mM 10-H2DA, which corresponds to the equivalent of around 37 g of crude RJ, indicating a secondary mechanism of action for anti-inflammatory pathways. In our experiments (utilizing between 10^5 and 10^7 RJEVs, equivalent to

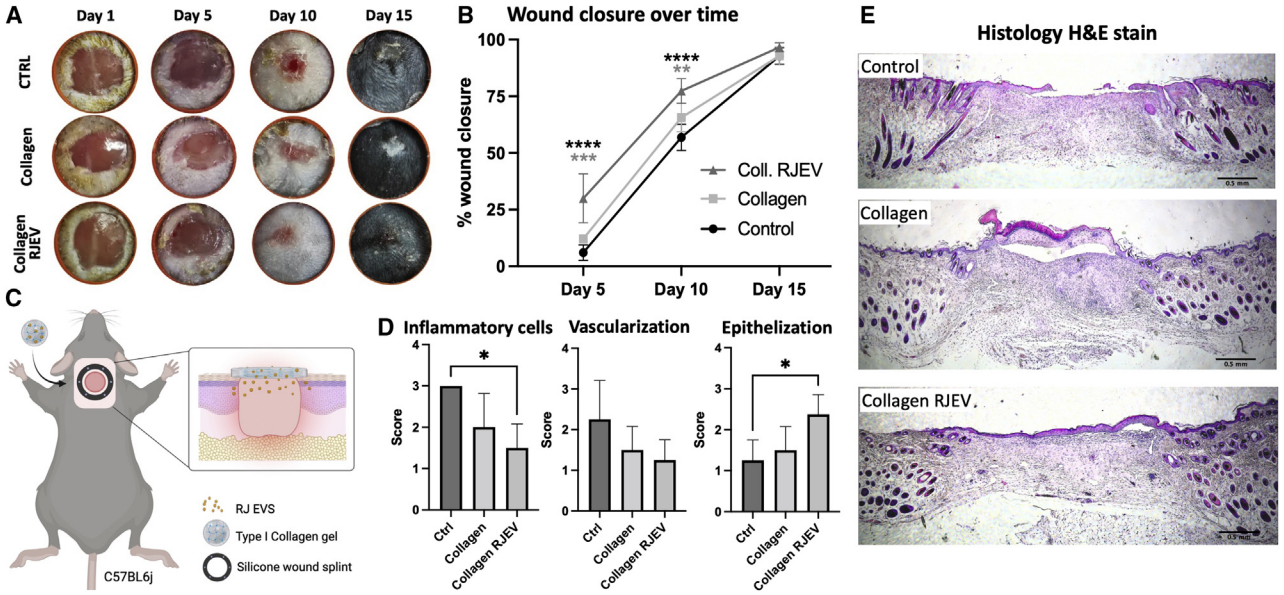

Figure 6. Effect of RJEVs in a mouse full-thickness splinted wound healing model

(A) Schematic of the wound healing model utilized; a full-thickness wound was inflicted in 10- to 12-week-old C57BL6 mice, and splinted with a silicone ring to avoid contraction; wounds were treated with type I collagen gels releasing RJEVs. (B) (i) Representative images of silicone splinted excision wounds at day 0, 5, 10, and 15. (B) (ii) Quantification of wound closure over time, displayed in percentage compared with day 0; n = 7; significance was tested with one-way ANOVA with Tukey's post hoc for differences between groups on different time points; *p < 0.05, **p < 0.01, ***p < 0.001, ****p < 0.0001; black asterisk displays difference to control, gray asterisk to collagen group. (D) (i) Histoscore quantification for inflammatory cells, vascularization, and epithelization; n = 4; significance was tested with one-way ANOVA with Tukey's post hoc for differences between groups on different time points; *p < 0.05; (E) (ii) Representative images of the wound tissues harvested on day 15, stained with hematoxylin-eosin; scale bar ≙ 500 μm. Data are shown as mean ± SD.

0.1–10 mg of crude RJ), we found a significant reduction in pro-inflammatory cytokine secretion for IL-1β, IL-6, and TNFα in the higher concentration, and for IL-6 and TNFα in the lower concentration (Figure 4A). Furthermore, we could verify the involvement of RJEVs in the inhibition of JNK and ERK1/2 phosphorylation (Figure 4B). The observed effects for RJEVs are comparable in magnitude and dosage with crude RJ, as reported by Kohno et al. for the same cell line (RAW 264.7),[17] indicating a stronger involvement of RJEVs in the anti-inflammatory effect of RJ as honeybee-specific fatty acids.

In the literature, the *in vivo* effects of RJ in wound healing models are well described and have been associated with an interplay of previously mentioned fatty acids, MRJP1, and antibacterial peptides such as defensin-1.[52] We hypothesized that RJEVs act as protection against degradation and transport vehicles for such proteins or peptides. In our previous study, we reported type I collagen as a suitable delivery matrix for RJEVs, displaying a stable release of functional RJEVs for at least 7 days.[22] Therefore, we tested RJEV antibacterial and pro-regenerative properties in separate animal models in order to comply with the 3R concept. Antibacterial assays were performed in a subcutaneous pocket, reducing the risk of systemic infection, and we observed strong bactericidal effects of RJEVs that were released from type-1 collagen gels. The observed results for RJEVs were comparable with previously reported *in vitro* effects for the same bacterial strain, *S. aureus* ATCC 25923,[53] while untreated control groups displayed substantial bacterial growth within the surgical pocket (Figure 5).

Regarding *in vivo* wound healing assays, RJEVs significantly accelerated initial wound closure compared with controls. However, no difference was observed at the end of the study (day 15) since all wounds were fully closed (Figure 6B). Similar effects were observed by Bucekova et al., utilizing honeybee defensin-1,[52] a peptide also identified within RJEVs (Figure 1C). The initial increase in tissue regeneration might be explained by RJEVs modulating the inflammatory phase, which is backed up by our prior *in vitro* findings associated to a significant increase in fibroblast and MSC migration,[22,53] bactericidal effects (Figure 5), modulation of the tissue-resident MSC secretome (Figure 3), and modulation of LPS-stimulated immune responses (Figure 4). The advanced wound healing state can further be observed in the decrease of inflammatory cells and the increase of epithelial cells (Figure 6C). While a shortening of the inflammatory phase has only minor effects on physiological wound healing, it plays a crucial role in chronic wounds that are prone to prolonged inflammation.[54] Interestingly, even though *in vitro* MSCs secreted significantly more VEGF in the presence of RJEVs (Figure 3D), no significant effect was found on angiogenesis and the presence of newly formed blood vessels, with a trend toward a lower amount present in the RJEV group. It can be hypothesized that the increase in secretion might not be enough to trigger a substantial response *in vivo*;

however, endothelial cells are not the only cells responsive to VEGF. Non-traditional effects of VEGF include the stimulation of keratinocyte proliferation and migration and, as a result, promotion of wound re-epithelialization.[55,56] Furthermore, it has been shown that vessel density displays a peak during the proliferative phase, and subsequently decreases gradually.[57] Since wound closure occurs earlier in the RJEV group, the observed effect could also be explained by a slightly earlier onset of the remodeling phase.

Conclusions

Summarizing, we have gained first insights into the biogenesis of RJEVs by confirming the presence of the exosomal markers CD63 and syntenin and found that RJEVs carry important active cargo proteins such as MRJP1, defensin-1, and jellein-3. RJEV uptake analysis revealed a potential double mechanism of action within the cell, with the direct release of cargo into the cytoplasm after membrane fusion and intracellular sorting after macropinocytosis or clathrin-dependent endocytosis. Furthermore, RJEVs have been demonstrated to modulate MSCs on several levels (e.g., differentiation, proliferation, secretome) as well as LPS-induced inflammation in macrophages. In *in vivo* studies, we confirmed the known antibacterial effects of RJEVs, and discovered an acceleration of wound healing in a splinted mouse model. Overall, RJ is a highly complex bee product that has been of interest for medical applications for decades. In the last years, several active compounds have been discovered and RJEVs appear to be the missing link elucidating some of the as-yet unexplained effects. Further studies are needed, not only for potential medical application of RJEVs but also for basic research on honeybee cell functions, in order to understand the biogenesis, uptake, and the roles of RJEVs for honeybees themselves.

MATERIALS AND METHODS

Unless otherwise noted, all reagents were obtained from Sigma-Aldrich (US) and are of analytical grade. All cell culture assays were performed under standard cell culture conditions (37°C, 5% CO_2).

EV isolation and characterization

Exosome isolation was performed as previously described.[21] Briefly, RJ (Apicola del Alba, Chile) was diluted in particle-free phosphate buffered saline 1:40 (pf-PBS) and incubated for 30 min on an orbital shaker. Subsequently, debris was removed by serial centrifugation (500–2,000 × *g*, 15 min each) and filtered using a 0.2-μm polystyrene filter. Finally, the supernatant was ultra-centrifuged at 100,000 × *g* for 60 min (Hanil 5 fixed rotor ultracentrifuge, Hanil, Korea). The resulting pellet was resuspended in pf-PBS and stored at 80°C until further use.

Nanoparticle tracking analysis

As an initial step, particle quantification and size distribution were determined using nanoparticle tracking analysis (NTA). RJEV samples were thawed shortly before NTA, diluted 1:100 with pf-PBS, and vortexed three times for 1 s. Samples were measured five times using temperature control (25°C) at camera level 8 for 60 s (NanoSight NS 3000, Malvern, UK).

AFM characterization

RJEV shapes were confirmed using AFM, as previously described.[58] Briefly, freshly cleaved mica discs (12-mm diameter; Electron Microscopy Sciences, US) were coated with 50 μL of a 0.1 M solution of poly-L-lysine (PLL) for 5 min. Subsequently, discs were washed three times with double-distilled H_2O (ddH_2O) and dried with a gentle stream of N_2. RJEVs were then immobilized onto the PLL-coated mica by incubation for 30 min at room temperature. Samples were covered to avoid drying and potential dust contamination. After incubation, specimens were washed three times with ddH_2O and mounted onto an Asylum MFP 3D-SA AFM (Asylum Research, US). Samples were analyzed in intermittent contact mode (alternating current [AC] mode) with TAP300GD-G cantilevers (BudgetSensors, Bulgaria), obtaining height, amplitude, and phase channel images of substrates under environmental conditions. From the resulting height images, the surface profiles, maximum and mean vesicle height, and RMS roughness of RJEVs were calculated in the Gwyddion 2.56 software. RJEVs from three independent sample preparations were utilized for all AFM-based experiments.

Exosomal markers and cargo

To verify the exosomal origin, RJEVs were analyzed for the presence of CD63 and syntenin using western blot. For cargo analysis (MRJP1), RJEVs were sonicated for 15 min before analysis. Proteins were separated in reducing conditions (syntenin, MRJP1) and non-reducing conditions (CD63) utilizing a 10% polyacrylamide gel and blotted onto nitrocellulose. After blocking with 3% bovine serum albumin (BSA) in Tris-buffered saline with 0.1% Tween (TBS-T), membranes were incubated with the respective antibodies (anti-CD63, 1:500, mouse monoclonal, Abcam ab59479; anti-syntenin, 1:1,000, rabbit polyclonal, Abcam ab19903; anti- MRJP1, 1:1,000, rabbit polyclonal, Cusabio CSB-PA522725EA01DNK; 3% BSA TBS-T) overnight. Subsequently, membranes were thoroughly washed and incubated with secondary antibody (IR-Dye anti-mouse, 1:15,000, LiCor; IR-Dye anti-rabbit, 1:15,000, LiCor) in 3% BSA TBS-T for 1 h. Finally, membranes were revealed using an Odyssey CLx imaging system, and results were analyzed with Image Studio Digits version 5.2.5.

Furthermore, the peptides defensin-1 and jellein-3 were quantified with direct ELISA, as previously described.[58] Briefly, 1 μg of RJEV protein and negative controls (pre-bleed serum 1:1,000, human MSC protein 30 μg) and respective standards were incubated overnight. After blocking with 5% BSA, plates were incubated with respective detection antibodies diluted in reagent diluent (R&D systems) (anti-*A. mellifera* defensin-1, 50 ng/mL; rabbit polyclonal, GeneCust; anti-*A. mellifera* jellein-3; 50 ng/mL, rabbit polyclonal, GeneCust) for 2 h. Horseradish peroxidase (HRP)-conjugated anti-rabbit antibody was used at a dilution of 1:1,000 (Cell signaling, UK) and developed for 10 min using substrate solution (R&D systems). The reaction was stopped with 2 N H_2SO_4, and plates were measured using a microplate reader (Tecan Sunrise, Tecan, Austria) at 450 nm.

Effects on MSCs

For all experiments utilizing MSCs, written informed consent was obtained before MSC isolation and the protocols used were approved by the Ethics Committee of the Universidad del Desarrollo. MSCs derived from adipose tissue were cultivated in minimum essential medium (αMEM, Gibco, US) supplemented with 10% fetal bovine serum (FBS, HyClone, GE Healthcare, US), 200 mmol/L of L-glutamine (L-G), and 1% (v/v) penicillin-streptomycin (P/S) (standard culture medium). For the experimental group, RJEV preconditioned MSCs, cells were seeded at a density of 4×10^3 per cm^2 and incubated with 2.5×10^2 RJEVs per cell for 48 h. Subsequently, cells were transferred to the corresponding experiments without further addition of RJEVs.

Routes of RJEV uptake

To assess routes of uptake into mammalian cells, an uptake inhibition assay was performed. Prior to the assay, a cytotoxicity assay was performed to exclude effects on cell viability by the inhibitors (results in Figure S2). RJEVs were stained with fluorescent dye carboxyfluorescein succinimidyl ester (Cell Trace CFSE, Thermo Fisher Scientific), as previously described.[53] Human adipose-derived MSCs were seeded at a density of 5,000 cells per cm^2 in a six-well plate and left to adhere overnight. Each potential uptake route was blocked with either omeprazole 1 mM, amiloride 50 μM, chlorpromazine 28 μM, or filipin 7.5 μM (for 15 min). Cells were subsequently incubated with 2.5×10^3 CFSE-RJ-EVs per cell for 4 h and analyzed with flow cytometry (CyAn ADP, Beckman Coulter, US). Treatment groups were compared with unstained control as well as CFSE-RJ-EVs without inhibitor. FlowJo software (TreeStar, version 8.8.6) was used for data analysis.

PDT

To assess the effects of RJEVs on PDT, MSCs were seeded at an exact density (3.3×10^3 per cm^2) and left to adhere for 1 h, followed by adding 2.5×10^2 RJEVs per cell at every passage (RJEV group). Cells were counted after 120 h and reseeded at the same density until passage 13. Calculation was done with the following formula: PDT in days = ((time in days) × log (2))/(log (final cell number) × log (initial cell number)).

Secretory protein profile

To assess changes in the secretory profile of MSCs in the presence of RJEVs, four proteins involved in wound healing were selected for analysis: fibroblast growth factor (FGF), vascular endothelial growth factor (VEGF), insulin-like grwoth factor 1a (IGF-1a), and hepatocyte grwoth factor (HGF). Briefly, 10^3 cells per cm^2 were seeded in a six-well plate and left to adhere overnight. For conditioning, cells were cultivated in media without FBS. Supernatants were collected after 24 h, centrifuged at 1,000 × *g* for 15 min to remove cellular debris, and stored at −80°C until analysis. The respective proteins were quantified with sandwich ELISA (DuoSet, R&D Systems with ancillary kit) according to the manufacturer's instructions. Finally, the results were measured using a microplate reader (Tecan Sunrise, Tecan, Austria) at 450 nm.

Differentiation into adipogenic, osteogenic, and chondrogenic lineage

Cells were seeded at the respective cell densities for each differentiation assay (adipogenic lineage, $7.5 \times 10^3/cm^2$; osteogenic lineage, $5 \times 10^2/cm^2$; chondrogenic lineage, $7.5 \times 10^3/cm^2$; undifferentiated control, $5 \times 10^2/cm^2$) and were left to adhere overnight in standard culture medium. Subsequently, cells were incubated with respective differentiation media (StemPro adipogenic, osteogenic, chondrogenic differentiation kits; Gibco, US) for 14 days. An undifferentiated control was cultivated in standard culture medium supplemented with 5% FBS. RJEVs (10^6/well) were added, and each medium was changed every 3 days for 14 days. Adipogenic and osteogenic differentiation was evaluated using oil red O and Alizarin red staining, as previously described.[59] For chondrogenic differentiation, cells were fixed with ice-cold 70% methanol for 10 min at room temperature and stained with 0.1% Safranin O (w/v) for 10 min. For quantification, 200 μL of 100% ethanol was added to each well, and the plate was incubated for 30 min in an orbital shaker. Before quantification, representative images were taken on a Nikon Eclipse TS100. Quantification was performed using a microplate reader (Tecan Sunrise, Tecan, Austria).

Immune-modulatory assays

The immune-modulatory potential of RJEVs was assessed by employing the macrophage cell line RAW 264.7. Cells were cultivated using certified LPS-free Dulbecco's modified Eagle's medium and supplements (10% FBS, 200 mmol/L L-G, 1% P/S). For all immune-modulatory assays, cells were seeded at a density of 2×10^3 cells/cm^2. RJEVs were added at concentrations of 250/cell and 2.5×10^3/cell. For determining the secretory profile of pro-inflammatory cytokines (IL-1β, IL-6, and TNFα), RAW 264.7 cells were incubated with RJEVs for 12 h and subsequently stimulated with 1 μM LPS for 24 h. Supernatants were collected, centrifuged at 1,000 × *g* for 15 min to remove cellular debris, and stored at −80°C until analysis. Respective proteins were quantified with sandwich ELISA (DuoSet, R&D Systems with ancillary kit) according to the manufacturer's instructions. Results were measured using a microplate reader (Tecan Sunrise, Tecan, Austria) at 450 nm. For analysis of the associated pathways, RAW 264.7 cells were incubated with RJEVs for 12 h and subsequently stimulated with 1 μM LPS for 6 h. Cells were lysed using radio-immunoprecipitation assay buffer (RIPA buffer) for 15 min on ice, centrifuged at 10,000 × *g* to remove cellular debris, transferred to another tube, and stored at −20°C until further analysis. For western blot, proteins were quantified using a bicinchoninic acid assay (BCA assay). Proteins were separated in a 10% polyacrylamide gel, blotted onto nitrocellulose membranes, and blocked with 3% BSA-TBS-T. Membranes were incubated with the phosphorylated antibodies before unphosphorylated (antibodies Cell Signaling: extracellular signal-regulated kinase (ERK 1/2) #9102; phosho-ERK 1/2 #4370; Jun n-terminal kinase (JNK) #9252; phosphor JNK #4668; all 1:1000). Membranes were then thoroughly washed and incubated with secondary antibody (IR-Dye anti-mouse, 1:15,000, LiCor; IR-Dye anti-rabbit, 1:15,000, LiCor) in 3% BSA TBS-T for 1 h. Membranes were revealed using an Odyssey CLx imaging system, and results were analyzed with Image Studio Digits version 5.2.5.

Effects of RJEVs *in vivo*

All experimental procedures were approved by the local animal committee in accordance with the Chilean law, ARRIVE guidelines, and 3R practices (Replacement, Reduction and Refinement). C57BL/6 mice were kept in an enriched environment with a 12 h/12 h light/dark cycle, at 23°C–25°C ambient temperature, and food as well as water *ad libitum*. For experimentation, 10- to 12-week-old male and female mice with a minimum weight of 20 g were utilized. The well-being of animals was assessed daily using a Grimace scale as well as Morton and Griffith assessment. In all *in vivo* experiments, RJEVs were administered using a collagen type I hydrogel as previously described.[22] Briefly, 24 h before experimentation, collagen from rat tail (2 mg/mL in hydrochloric acid; Gibco, US) was mixed with 10 × MEM (Gibco, US) in a ratio of 8:1. Gelation was induced by neutralization with 1 M sodium hydroxide and one part RJEVs was added at a concentration of 5×10^9/mL. Control gels not carrying RJEVs were adjusted with one part PBS. The resulting solution was transferred into a 96-well plate (100 µL) and incubated at 37°C for 30 min. Subsequently, gels were covered with 100 µL of PBS.

In vivo *antibacterial properties*

Before surgery, *S. aureus* ATCC 25923 cells were activated in brain heart infusion (BHI) broth at 37°C and 150 rpm orbital shaking for 5 h and adjusted to 0.5 McFarland directly before experiments. Mice were randomly assigned to respective groups (control, *S. aureus* control, collagen control, collagen RJEV) and deeply anesthetized using sevoflurane by inhalation. After hair removal on both sides of the dorsum, the area was disinfected with povidone-iodine to avoid contamination. A 5-mm incision was made on both sides of the dorsum, and undermining was performed to create a small pocket. Collagen gels (collagen control, collagen RJEV) were cut in half to create a semilunar shape (2.5 × 4 × 1 mm) and placed inside the pocket. To the control, collagen control, and collagen RJEV groups, 5 µL of bacterial solution were added. Sham received 5 µL of saline solution. Surgical sites were closed with 5.0 Vicryl sutures. Mice were given analgesics (meloxicam, 2 mg/kg) after the surgery and the following day. Forty-eight hours after surgery, mice were euthanized, and incision sites were opened. Using a sterile loop, bacteria were collected from the pocket and placed in 1 mL of BHI broth. Subsequently, bacteria were plated in serial dilution on BHI agar plates for colony counts and in 96-well plates (100µL of BHI broth) for viability assays. After overnight incubation, colonies were counted on agar plates. For viability quantification, resazurin 0.016% was added to the wells for 1 h at 37°C and was subsequently measured at 570 nm in a microplate reader.

Mouse full-thickness wound healing model

Mice were randomly assigned to respective groups (control, collagen control, collagen RJEV) and deeply anesthetized using sevoflurane by inhalation. The center part of the dorsum was depilated around the neck and disinfected with povidone-iodine. Subsequently, a 5-mm full-thickness wound was created using a sterile histopunch. A silicone wound splint (15 mm/7 mm outer/inner diameter, Grace Biolabs, UK) was centered on the wound area and fixed with skin adhesive as well as six sutures (Vicryl 5.0). Collagen gels were placed on the fresh wound, and the area was covered with Tegaderm (3M, US). Mice were given analgesics (meloxicam, 2 mg/kg) once a day for the 3 days after surgery. Collagen gels were replaced every 5 days and the wound area was covered again with Tegaderm. Pictures were taken directly after surgery and on days 5, 10, and 15. Wound closure was measured using ImageJ software and calculated compared with day 0. On day 15, mice were euthanized and tissue was harvested and fixed (4% formaldehyde) for 48 h. For histological analysis, tissues were embedded in paraffin using standard protocols, and 5-µm sections were stained with hematoxylin-eosin to assess re-epithelization, vascularization, and inflammation using a scoring system, as described by de Moura Estevao et al.[60]

Statistics

All data in this study are shown as mean ± standard deviation. All data were tested for normality using the Shapiro-Wilk test. Statistical analysis was performed using Student's t test (for two groups) or one-way ANOVA followed by Tukey's range test for significant differences between means (for three or more groups). Two-way ANOVA with Šídák's multiple comparisons test was used for time course analysis. Analysis was performed using GraphPad Prism 9 for Mac OS X, version 9.3.1 (GraphPad Software). Significance was considered at $p < 0.05$ (see figure legends for specific values). N values were determined from independent experiments and independent isolations of RJEVs.

DATA AVAILABILITY

The datasets used and/or analyzed during the current study are available from the corresponding author on request.

SUPPLEMENTAL INFORMATION

Supplemental information can be found online at https://doi.org/10.1016/j.omtn.2023.02.008.

ACKNOWLEDGMENTS

This work was financially supported by the independent funding agency ANID Chile (Agencia Nacional de Investigación y Desarrollo), under the grant scheme FONDECYT Iniciación (#11180406), and FONDECYT regular (#1220803 and #1220804). We would like to thank Pia Schuh for inspiring this research. Furthermore, we would like to thank Luis Délano for his help and support with the histological samples.

AUTHOR CONTRIBUTIONS

S.A., P.C.-K., and S.A. contributed equally to data acquisition, analysis and interpretation, manuscript drafting, and critically revising the final manuscript. O.R., C.V., J.R., L.D., and B.M. contributed to data acquisition and analysis, and critically revised the manuscript. C.S. designed the study and contributed to data acquisition, analysis and interpretation, manuscript drafting, and critically revising of the final manuscript. All authors have read and approved the current version of the manuscript.

DECLARATION OF INTERESTS

The authors declare no competing interests.

REFERENCES

1. Bessa, L.J., Fazii, P., Di Giulio, M., and Cellini, L. (2015). Bacterial isolates from infected wounds and their antibiotic susceptibility pattern: some remarks about wound infection. Int. Wound J. *12*, 47–52. https://doi.org/10.1111/iwj.12049.
2. Frykberg, R.G., and Banks, J. (2015). Challenges in the treatment of chronic wounds. Adv. Wound Care *4*, 560–582. https://doi.org/10.1089/wound.2015.0635.
3. Raposo, G., Nijman, H.W., Stoorvogel, W., Liejendekker, R., Harding, C.V., Melief, C.J., and Geuze, H.J. (1996). B lymphocytes secrete antigen-presenting vesicles. J. Exp. Med. *183*, 1161–1172. https://doi.org/10.1084/jem.183.3.1161.
4. Valadi, H., Ekström, K., Bossios, A., Sjöstrand, M., Lee, J.J., and Lötvall, J.O. (2007). Exosome-mediated transfer of mRNAs and microRNAs is a novel mechanism of genetic exchange between cells. Nat. Cell Biol. *9*, 654–659. https://doi.org/10.1038/ncb1596.
5. Schuh, C.M.A.P., Cuenca, J., Alcayaga-Miranda, F., and Khoury, M. (2019). Exosomes on the border of species and kingdom intercommunication. Transl. Res. *210*, 80–98. https://doi.org/10.1016/j.trsl.2019.03.008.
6. Moore, A.R. (1976). Man and wound in the ancient world. Med. J. Aust. *2*, 422–423. https://doi.org/10.1086/352029.
7. Ahmed, A.K.J., Hoekstra, M.J., Hage, J.J., and Karim, R.B. (2003). Honey-medicated dressing: transformation of an ancient remedy into modern therapy. Ann. Plast. Surg. *50*, 143–147. , discussion 147-148. https://doi.org/10.1097/01.SAP.0000032306.44107.C1.
8. Fratini, F., Cilia, G., Mancini, S., and Felicioli, A. (2016). Royal Jelly: an ancient remedy with remarkable antibacterial properties. Microbiol. Res. *192*, 130–141. https://doi.org/10.1016/j.micres.2016.06.007.
9. Suemaru, K., Cui, R., Li, B., Watanabe, S., Okihara, K., Hashimoto, K., Yamada, H., and Araki, H. (2008). Topical application of royal jelly has a healing effect for 5-fluorouracil-induced experimental oral mucositis in hamsters. Methods Find. Exp. Clin. Pharmacol. *30*, 103–106. https://doi.org/10.1358/mf.2008.30.2.1159655.
10. Karaca, T., Bayiroglu, F., Yoruk, M., Kaya, M.S., Uslu, S., Comba, B., and Mis, L. (2010). Effect of royal jelly on experimental colitis induced by acetic acid and alteration of mast cell distribution in the colon of rats. Eur. J. Histochem. *54*, e35. https://doi.org/10.4081/ejh.2010.e35.
11. Özan, F., Çörekçi, B., Toptaş, O., Halicioğlu, K., Irgin, C., Yilmaz, F., and Hezenci, Y. (2015). Effect of Royal Jelly on new bone formation in rapid maxillary expansion in rats. Med. Oral Patol. Oral Cir. Bucal *20*, e651–e656. https://doi.org/10.4317/medoral.20581.
12. El-Gayar, M.H., Aboshanab, K.M., Aboulwafa, M.M., and Hassouna, N.A. (2016). Antivirulence and wound healing effects of royal jelly and garlic extract for the control of MRSA skin infections. Wound Med. *13*, 18–27. https://doi.org/10.1016/j.wndm.2016.05.004.
13. Siavash, M., Shokri, S., Haghighi, S., Shahtalebi, M.A., and Farajzadehgan, Z. (2015). The efficacy of topical royal jelly on healing of diabetic foot ulcers: a double-blind placebo-controlled clinical trial. Int. Wound J. *12*, 137–142. https://doi.org/10.1111/iwj.12063.
14. Yanagita, M., Kojima, Y., Mori, K., Yamada, S., and Murakami, S. (2011). Osteoinductive and anti-inflammatory effect of royal jelly on periodontal ligament cells. Biomed. Res. *32*, 285–291. JST.JSTAGE/biomedres/32.285 [pii].
15. Hattori, N., Nomoto, H., Fukumitsu, H., Mishima, S., and Furukawa, S. (2007). Royal jelly and its unique fatty acid, 10-hydroxy-trans-2-decenoic acid, promote neurogenesis by neural stem/progenitor cells in vitro. Biomed. Res. *28*, 261–266. https://doi.org/10.2220/biomedres.28.261.
16. Kim, J., Kim, Y., Yun, H., Park, H., Kim, S.Y., Lee, K.-G., Han, S.-M., and Cho, Y. (2010). Royal jelly enhances migration of human dermal fibroblasts and alters the levels of cholesterol and sphinganine in an *in vitro* wound healing model. Nutr. Res. Pract. *4*, 362–368. https://doi.org/10.4162/nrp.2010.4.5.362.
17. Kohno, K., Okamoto, I., Sano, O., Arai, N., Iwaki, K., Ikeda, M., and Kurimoto, M. (2004). Royal jelly inhibits the production of proinflammatory cytokines by activated macrophages. Biosci. Biotechnol. Biochem. *68*, 138–145. https://doi.org/10.1271/bbb.68.138.
18. Okamoto, I., Taniguchi, Y., Kunikata, T., Kohno, K., Iwaki, K., Ikeda, M., and Kurimoto, M. (2003). Major royal jelly protein 3 modulates immune responses in vitro and in vivo. Life Sci. *73*, 2029–2045. https://doi.org/10.1016/S0024-3205(03)00562-9.
19. Natarajan, O., Angeloni, J.T., Bilodeau, M.F., Russi, K.E., Dong, Y., and Cao, M. (2021). The immunomodulatory effects of royal jelly on defending against bacterial infections in the Caenorhabditis elegans model. J. Med. Food *24*, 358–369. https://doi.org/10.1089/jmf.2020.0050.
20. Mccleskey, C.S., and Melampy, R.M. (1939). Bactericidal properties of royal jelly of the honeybee 1. J. Econ. Entomol. *32*, 581–587. https://doi.org/10.1093/jee/32.4.581.
21. Schuh, C.M.A.P., Aguayo, S., Zavala, G., and Khoury, M. (2019). Exosome-like vesicles in Apis mellifera bee pollen, honey and royal jelly contribute to their antibacterial and pro-regenerative activity. J. Exp. Biol. *222*, jeb208702. https://doi.org/10.1242/jeb.208702.
22. Ramírez, O.J., Alvarez, S., Contreras-Kallens, P., Barrera, N.P., Aguayo, S., and Schuh, C.M.A.P. (2020). Type I collagen hydrogels as a delivery matrix for royal jelly derived extracellular vesicles. Drug Deliv. *27*, 1308–1318. https://doi.org/10.1080/10717544.2020.1818880.
23. Chopra, N., Dutt Arya, B., Jain, N., Yadav, P., Wajid, S., Singh, S.P., and Choudhury, S. (2019). Biophysical characterization and drug delivery potential of exosomes from human Wharton's jelly-derived mesenchymal stem cells. ACS Omega *4*, 13143–13152. https://doi.org/10.1021/acsomega.9b01180.
24. Pietrangelo, T., Di Filippo, E.S., Locatelli, M., Piacenza, F., Farina, M., Pavoni, E., Di Donato, A., Innosa, D., Provinciali, M., and Fulle, S. (2018). Extracellular guanosine 5′-triphosphate induces human muscle satellite cells to release exosomes stuffed with guanosine. Front. Pharmacol. *9*, 152.
25. Cheng, J., Nonaka, T., and Wong, D.T.W. (2019). Salivary exosomes as nanocarriers for cancer biomarker delivery. Materials *12*, 654. https://doi.org/10.3390/ma12040654.
26. Dindia, L., Murray, J., Faught, E., Davis, T.L., Leonenko, Z., and Vijayan, M.M. (2012). Novel nongenomic signaling by glucocorticoid may involve changes to liver membrane order in rainbow trout. PLoS One *7*, e46859. https://doi.org/10.1371/journal.pone.0046859.
27. Raposo, G., and Stoorvogel, W. (2013). Extracellular vesicles: exosomes, microvesicles, and friends. J. Cell Biol. *200*, 373–383. https://doi.org/10.1083/jcb.201211138.
28. Stoorvogel, W. (2015). Resolving sorting mechanisms into exosomes. Cell Res. *25*, 531–532. https://doi.org/10.1038/cr.2015.39.
29. David, G., and Zimmermann, P. (2016). Heparanase tailors syndecan for exosome production. Mol. Cell. Oncol. *3*, e1047556. https://doi.org/10.1080/23723556.2015.1047556.
30. Honda, Y., Araki, Y., Hata, T., Ichihara, K., Ito, M., Tanaka, M., and Honda, S. (2015). 10-Hydroxy-2-decenoic acid, the major lipid component of royal jelly, extends the lifespan of Caenorhabditis elegans through dietary restriction and target of rapamycin signaling. J. Aging Res. *2015*, 425261. https://doi.org/10.1155/2015/425261.
31. Lin, Y., Zhang, M., Wang, L., Lin, T., Wang, G., Peng, J., and Su, S. (2020). The in vitro and in vivo wound-healing effects of royal jelly derived from Apis mellifera L. during blossom seasons of Castanea mollissima Bl. and Brassica napus L. in South China exhibited distinct patterns. BMC Complement. Med. Ther. *20*, 357. https://doi.org/10.1186/s12906-020-03138-5.
32. Garcia, M.C., Finola, M.S., and Marioli, J.M. (2013). Bioassay directed identification of royal jelly's active compounds against the growth of bacteria capable of infecting cutaneous wounds. Adv. Microbiol. *03*, 138–144. https://doi.org/10.4236/aim.2013.32022.
33. Moselhy, W.A., Fawzy, A.M., and Kamel, A.A. (2013). An evaluation of the potent antimicrobial effects and unsaponifiable matter analysis of the royal jelly. Life Sci. J. *10*, 290–296.
34. Ratanavalachai, T., and Wongchai, V. (2002). Antibacterial activitv of intact roval jelly , its lipid extract and its defatted extract. Thammasat Int. J. Sci. Technol. *7*, 5–12.

35. Fujiwara, S., Imai, J., Fujiwara, M., Yaeshima, T., Kawashima, T., and Kobayashi, K. (1990). A potent antibacterial protein in royal jelly. Purification and determination of the primary structure of royalisin. J. Biol. Chem. *265*, 11333–11337.

36. Fontana, R., Mendes, M.A., De Souza, B.M., Konno, K., César, L.M.M., Malaspina, O., and Palma, M.S. (2004). Jelleines: a family of antimicrobial peptides from the Royal Jelly of honeybees (Apis mellifera). Peptides *25*, 919–928. https://doi.org/10.1016/j.peptides.2004.03.016.

37. Eshraghi, S. (2005). An evaluation of the potent inhibitory effects of royal jelly fractions against Streptomyces bacteria. Pakistan J. Med. Sci. *21*, 63–68.

38. Wan, D.C., Morgan, S.L., Spencley, A.L., Mariano, N., Chang, E.Y., Shankar, G., Luo, Y., Li, T.H., Huh, D., Huynh, S.K., et al. (2018). Honey bee Royalactin unlocks conserved pluripotency pathway in mammals. Nat. Commun. *9*, 5078. https://doi.org/10.1038/s41467-018-06256-4.

39. Schuh, C.M.A.P., Heher, P., Weihs, A.M., Banerjee, A., Fuchs, C., Gabriel, C., Wolbank, S., Mittermayr, R., Redl, H., Rünzler, D., and Teuschl, A.H. (2014). In vitro extracorporeal shock wave treatment enhances stemness and preserves multipotency of rat and human adipose-derived stem cells. Cytotherapy *16*, 1666–1678. https://doi.org/10.1016/j.jcyt.2014.07.005.

40. Nekanti, U., Mohanty, L., Venugopal, P., Balasubramanian, S., Totey, S., and Ta, M. (2010). Optimization and scale-up of Wharton's jelly-derived mesenchymal stem cells for clinical applications. Stem Cell Res. *5*, 244–254. https://doi.org/10.1016/j.scr.2010.08.005.

41. Lee, M.-S., Youn, C., Kim, J.H., Park, B.J., Ahn, J., Hong, S., Kim, Y.-D., Shin, Y.K., and Park, S.G. (2017). Enhanced cell growth of adipocyte-derived mesenchymal stem cells using chemically-defined serum-free media. Int. J. Mol. Sci. *18*, 1779. https://doi.org/10.3390/ijms18081779.

42. Garoufalia, Z., Papadopetraki, A., Karatza, E., Vardakostas, D., Philippou, A., Kouraklis, G., and Mantas, D. (2021). Insulin-like growth factor-I and wound healing, a potential answer to non-healing wounds: a systematic review of the literature and future perspectives. Biomed. Rep. *15*, 66. https://doi.org/10.3892/br.2021.1442.

43. Shi, H.-X., Lin, C., Lin, B.-B., Wang, Z.-G., Zhang, H.-Y., Wu, F.-Z., Cheng, Y., Xiang, L.-J., Guo, D.-J., Luo, X., et al. (2013). The anti-scar effects of basic fibroblast growth factor on the wound repair in vitro and in vivo. PLoS One *8*, e59966.

44. Ishiguro, S., Akasaka, Y., Kiguchi, H., Suzuki, T., Imaizumi, R., Ishikawa, Y., Ito, K., and Ishii, T. (2009). Basic fibroblast growth factor induces down-regulation of α-smooth muscle actin and reduction of myofibroblast areas in open skin wounds. Wound Repair Regen. *17*, 617–625. https://doi.org/10.1111/j.1524-475X.2009.00511.x.

45. Matsumoto, K., Hashimoto, K., Yoshikawa, K., and Nakamura, T. (1991). Marked stimulation of growth and motility of human keratinocytes by hepatocyte growth factor. Exp. Cell Res. *196*, 114–120. https://doi.org/10.1016/0014-4827(91)90462-4.

46. Dunsmore, S.E., Rubin, J.S., Kovacs, S.O., Chedid, M., Parks, W.C., and Welgus, H.G. (1996). Mechanisms of hepatocyte growth factor stimulation of keratinocyte metalloproteinase production. J. Biol. Chem. *271*, 24576–24582. https://doi.org/10.1074/jbc.271.40.24576.

47. Li, J.-F., Duan, H.-F., Wu, C.-T., Zhang, D.-J., Deng, Y., Yin, H.-L., Han, B., Gong, H.-C., Wang, H.-W., and Wang, Y.-L. (2013). HGF accelerates wound healing by promoting the dedifferentiation of epidermal cells through β1-integrin/ILK pathway. BioMed Res. Int. *2013*, 470418. https://doi.org/10.1155/2013/470418.

48. Bao, P., Kodra, A., Tomic-Canic, M., Golinko, M.S., Ehrlich, H.P., and Brem, H. (2009). The role of vascular endothelial growth factor in wound healing. J. Surg. Res. *153*, 347–358. https://doi.org/10.1016/j.jss.2008.04.023.

49. You, M.M., Chen, Y.F., Pan, Y.M., Liu, Y.C., Tu, J., Wang, K., and Hu, F.L. (2018). Royal jelly attenuates LPS-induced inflammation in BV-2 microglial cells through modulating NF-κB and p38/JNK signaling pathways. Mediators Inflamm. *2018*, 7834381. https://doi.org/10.1155/2018/7834381.

50. Chen, Y.-F., Wang, K., Zhang, Y.-Z., Zheng, Y.-F., and Hu, F.-L. (2016). In vitro anti-inflammatory effects of three fatty acids from royal jelly. Mediators Inflamm. *2016*, 1–11. https://doi.org/10.1155/2016/3583684.

51. Balkanska, R. (2018). Determination of trans-10-hydroxy-2-decenoic acid in royal jelly by high performance liquid chromatography after different bee feeding. Int. J. Curr. Microbiol. Appl. Sci. *7*, 3738–3743. https://doi.org/10.20546/ijcmas.2018.704.420.

52. Bucekova, M., Sojka, M., Valachova, I., Martinotti, S., Ranzato, E., Szep, Z., Majtan, V., Klaudiny, J., and Majtan, J. (2017). Bee-derived antibacterial peptide, defensin-1, promotes wound re-epithelialisation in vitro and in vivo. Sci. Rep. *7*, 7340. https://doi.org/10.1038/s41598-017-07494-0.

53. Schuh, C.M.A.P., Aguayo, S., Zavala, G., and Khoury, M. (2019). Exosome-like vesicles in Apis mellifera bee pollen, honey and royal jelly contribute to their antibacterial and pro-regenerative activity. J. Exp. Biol. *222*, jeb208702. https://doi.org/10.1242/jeb.208702.

54. Schilrreff, P., and Alexiev, U. (2022). Chronic inflammation in non-healing skin wounds and promising natural bioactive compounds treatment. Int. J. Mol. Sci. *23*, 4928. https://doi.org/10.3390/ijms23094928.

55. Wilgus, T.A., Matthies, A.M., Radek, K.A., Dovi, J.V., Burns, A.L., Shankar, R., and DiPietro, L.A. (2005). Novel function for vascular endothelial growth factor receptor-1 on epidermal keratinocytes. Am. J. Pathol. *167*, 1257–1266. https://doi.org/10.1016/S0002-9440(10)61213-8.

56. Man, X.-Y., Yang, X.-H., Cai, S.-Q., Yao, Y.-G., and Zheng, M. (2006). Immunolocalization and expression of vascular endothelial growth factor receptors (VEGFRs) and neuropilins (NRPs) on keratinocytes in human epidermis. Mol. Med. *12*, 127–136. https://doi.org/10.2119/2006-00024.Man.

57. Johnson, A., and DiPietro, L.A. (2013). Apoptosis and angiogenesis: an evolving mechanism for fibrosis. FASEB J. Off. Publ. Fed. Am. Soc. Exp. Biol. *27*, 3893–3901. https://doi.org/10.1096/fj.12-214189.

58. Leiva-Sabadini, C., Alvarez, S., Barrera, N.P., Schuh, C.M.A.P., and Aguayo, S. (2021). Antibacterial effect of honey-derived exosomes containing antimicrobial peptides against oral streptococci. Int. J. Nanomed. *16*, 4891–4900. https://doi.org/10.2147/IJN.S315040.

59. Priglinger, E., Schuh, C.M.A.P., Steffenhagen, C., Wurzer, C., Maier, J., Nuernberger, S., Holnthoner, W., Fuchs, C., Suessner, S., Rünzler, D., et al. (2017). Improvement of adipose tissue-derived cells by low-energy extracorporeal shock wave therapy. Cytotherapy *19*, 1079–1095. https://doi.org/10.1016/j.jcyt.2017.05.010.

60. de Moura Estevão, L.R., Cassini-Vieira, P., Leite, A.G.B., de Carvalho Bulhões, A.A.V., da Silva Barcelos, L., and Evêncio-Neto, J. (2019). Morphological evaluation of wound healing events in the excisional wound healing model in rats. Bio. Protoc. *9*, e3285. https://doi.org/10.21769/bioprotoc.3285.